



Scholars' Mine

Masters Theses


Student Theses and Dissertations

Spring 2015

Computer aided detection of oral lesions on CT images

Shaikat Mahmood Galib

Follow this and additional works at: https://scholarsmine.mst.edu/masters_theses

 Part of the [Bioimaging and Biomedical Optics Commons](#), [Computer Engineering Commons](#), [Nuclear Engineering Commons](#), and the [Radiology Commons](#)

Department:

Recommended Citation

Galib, Shaikat Mahmood, "Computer aided detection of oral lesions on CT images" (2015). *Masters Theses*. 7395.

https://scholarsmine.mst.edu/masters_theses/7395

This thesis is brought to you by Scholars' Mine, a service of the Missouri S&T Library and Learning Resources. This work is protected by U. S. Copyright Law. Unauthorized use including reproduction for redistribution requires the permission of the copyright holder. For more information, please contact scholarsmine@mst.edu.

COMPUTER AIDED DETECTION OF ORAL LESIONS ON
CT IMAGES

by

SHAIKAT MAHMOOD GALIB

A THESIS

Presented to the Faculty of the Graduate School of the
MISSOURI UNIVERSITY OF SCIENCE AND TECHNOLOGY

In Partial Fulfillment of the Requirements for the Degree

MASTER OF SCIENCE IN NUCLEAR ENGINEERING

2015

Approved by

Hyoung Koo Lee, Advisor

Shoaib Usman

Ayodeji Babatunde Alajo

PUBLICATION THESIS OPTION

This thesis consists of the journal article that will be submitted for publication to Medical Image Analysis. Pages 1-31 of this thesis will be regenerated for writing the journal article on Medical Image Analysis.

ABSTRACT

Oral lesions are important findings on computed tomography images. They are difficult to detect on CT images because of low contrast, arbitrary orientation of objects, complicated topology and lack of clear lines indicating lesions. In this thesis, a fully automatic method to detect oral lesions from dental CT images is proposed to identify (1) Closed boundary lesions and (2) Bone deformation lesions. Two algorithms were developed to recognize these two types of lesions, which cover most of the lesion types that can be found on CT images. The results were validated using a dataset of 52 patients. Using non training dataset, closed boundary lesion detection algorithm yielded 71% sensitivity with 0.31 false positives per patient. Moreover, bone deformation lesion detection algorithm achieved 100% sensitivity with 0.13 false positives per patient. Results suggest that, the proposed framework has the potential to be used in clinical context, and assist radiologists for better diagnosis.

ACKNOWLEDGMENTS

I would like to express my heartfelt gratitude and sincere thanks to Dr. Hyoung Koo Lee, my advisor, whose guidance and direction greatly helped me through my Master's degree.

I would also like to thank my committee members, Dr. Shoaib Usman, for his support and advice about instructing the radiation detection and measurement laboratory, and Dr. Ayodeji Babatunde Alajo, for his insightful teaching about basics of nuclear engineering. I would also like to thank Vatech Co., Ltd, South Korea for funding this project and providing materials and information as needed.

I want to sincerely thank Fahima Islam for sharing her knowledge about image processing with me and helping me throughout the project. I also want to thank Muhammad Abir for his valuable advice and support in every aspect of my graduate studies, who made my life a lot easier abroad. I want to thank my friend Brendan D'souza for being supportive to me whenever I needed.

Most importantly, I would like to thank my mother, Momotaz Begum and my father, M. A. Khaleque, who always supported and encouraged me to do higher studies, and Fatema Binte Rasul, my wife, who was always beside me through this journey, through good or bad days. Without them none of this would have been possible.

TABLE OF CONTENTS

	Page
ABSTRACT.....	iv
ACKNOWLEDGMENTS	v
LIST OF ILLUSTRATIONS.....	viii
ABBREVIATIONS	ix
SECTION	
1. INTRODUCTION.....	1
2. RELATED WORKS	3
2.1. CARIES DIAGNOSIS.....	3
2.2. BONE DENSITY DIAGNOSIS.....	4
2.3. LESION/BONE DEFECT DIAGNOSIS.....	4
3. MATERIALS	6
4. METHODOLOGY.....	7
4.1. IMAGE PATTERN ANALYSIS.....	9
4.2. PREPROCESSING.....	10
4.3. DETECTION OF CLOSED BOUNDARY LESION (CBL) (TYPE I).....	11
4.3.1. Initial Lesion Candidates Detection	12
4.3.1.1. Binarization.....	12
4.3.1.2. Denoising	14
4.3.1.3. Blob detection	15
4.3.2. Feature Extraction	15
4.3.2.1. First order statistics.....	16
4.3.2.2. Second order statistics.....	16
4.3.2.3. Image moments.....	18
4.3.3. Classification	19
4.4. DETECTION OF BONE DEFORMATION (TYPE II)	23
4.5. DECISION MAKING AND LESION AREA MARKING	25
5. RESULTS AND DISCUSSION	26

5.1. EVALUATION OF CLOSED BOUNDARY LESION DETECTION ALGORITHM	27
5.2. EVALUATION OF BONE DEFORMATION DETECTION ALGORITHM.....	29
6. CONCLUSIONS	31
APPENDIX	32
REFERENCES	37
VITA	40

LIST OF ILLUSTRATIONS

Figure	Page
4.1. Illustration of two types of Lesions.	7
4.2. Architecture of the proposed method.....	8
4.3. An example plot of image pattern analysis.....	9
4.4. Illustration of all the CT slices (496) for a single patient.	10
4.5. Illustration of preprocessing process.	11
4.6. Block diagram of Closed boundary lesion detection method	12
4.7. Example of some automatic threshold methods	14
4.8. Illustration of denoising process	15
4.9. Illustration of blob detection process	16
4.10. Illustration of ROI extraction process.....	17
4.11. Configuration of multi layer perceptron neural network	20
4.12. Flow diagram of a single neuron	21
4.13. Illustrations of training samples.....	21
4.14. Training of Artificial neural network.....	22
4.15. Illustration of classification process by neural network	23
4.16. Illustration of Bone deformation lesion detection process.	24
5.1 Distribution of abnormal patient case dataset.....	26
5.2. Comparison of FROC curves in closed boundary lesion detection	28
5.3. FROC Curve of Bone deformation detection algorithm.....	30

ABBREVIATIONS

Acronyms	Description
CAD	Computer Aided Detection
CT	Computed Tomography
PET	Positron Emission Tomography
SPECT	Single-Photon Emission Computed Tomography
MRI	Magnetic Resonance Imaging
ROI	Region of Interest
ANN	Artificial Neural Network
GLCM	Grey-Level Co-occurrence Matrices
MLP	Multi Layer Perceptron
FROC	Free Response Receiver Operating Characteristics
TP	True Positive
FP	False Positive
TN	True Negative
FN	False Negative

1. INTRODUCTION

Computer Aided Detection (CAD) is a technology that is targeted to assist medical doctors for diagnosing and detecting diseases. CAD systems are usually developed for interpreting medical images (e.g. Radiography, MRI, Tomography, Ultrasound, PET, SPECT etc.) and providing second opinion to doctors. Study shows that a well-designed CAD system can increase medical doctor's performance and therefore reduce incorrect actions and diagnosis time [1]. Several CAD systems have been implemented commercially for detecting breast cancer, lung cancer, colon cancer, Alzheimer's disease and so on.

In this thesis, we are proposing a CAD system that is expected to detect oral lesions from dental CT images in mandibular region. According to the report of National Cancer Institute, oral cancer is accountable for 2.5% of all cancers in the United States [2]. Research shows, if oral cancer is detected in early stages, death rate can be reduced to 10% - 20% than later stages, which causes 40% - 65% death [2].

Dentists use different kinds of oral radiographs for distinct diagnostic purpose. Radiographs can be classified into two categories: Intraoral and Extraoral. In intraoral radiographs, film or sensor is placed inside the mouth to inspect the close view of a small area of the oral-maxillofacial region, whereas in extraoral radiographs, the film or sensor is placed outside of mouth to capture an overall view of the oral-maxillofacial region. CT imaging is a kind of extraoral radiograph which could be described as a series of x-ray images, each one a view of approximately 3mm section of the area being scanned. These sections are later combined together by a computer to produce a 3D view of the area. CT scan is commonly used for treatment planning of orthodontic issues, temporomandibular joint disorder diagnosis, correct placement of dental implants, evaluating the jaw, sinuses, nerve canals and nasal cavity; detecting, assessing and treating jaw tumors and many more [3]. Therefore, the added information of CT images enable doctors to diagnose a problem more accurately than the other type of radiographs.

Interpretation of dental CT images are challenging because image modalities are often poor due to noise, contrast is low and artifacts are present; topology is complicated; teeth orientation is arbitrary and lacks clear lines of separation between normal and

abnormal regions [4]. However, these inspections require dedicated training and dentist's time. Furthermore, the diagnosis may vary dentist to dentist, and experience plays a vital role in correct judgment and conclusion of diagnosis. Moreover, some early lesions may not be visible clearly to the human eye. These issues and their probable solutions are the primary motivation for this work. Therefore, it is intended to provide a better and effective diagnosing environment for dentists.

In this research, the prospects of an automated knowledge based CAD system for detecting oral lesions/abnormalities from CT images was investigated. However, dental CT images contain both maxilla and mandible of oral anatomy. Lesions of mandibular part only was studied in this work, and a method to detect its abnormalities was proposed. The suggested algorithm was an integration of image processing and pattern recognition techniques. The framework consists of two algorithms, one is for detection of closed boundary lesion (Type I) and the other is for detection of bone deformation (Type II). Image processing involved in these two algorithms were implemented in 2D CT slice images and final decision was made by analyzing the results in a 3D CT volume. These two algorithms were combined together to highlight a suspicious region for further assessment of a dentist. This thesis reports the methodology and finally evaluates the results to validate the goal of a CAD system.

2. RELATED WORKS

Computerized dental treatment systems and clinical decision support systems have seen success in recent years. Many diverse CAD systems were developed for diagnosing different oral diseases. Based on most researched cases, we have broadly classified the research areas into three different categories: caries diagnosis, bone density diagnosis and lesion/bone defect diagnosis. Following sections describe the categories in short.

2.1. CARIES DIAGNOSIS

Computer aided caries diagnosis technology is perhaps the most studied category in the dental radiograph analysis field. The Logicon® System (Carestream Dental LLC, Atlanta, GA) is a well-known technology for caries detection [5]. This software has a database which contains teeth with matching clinical images, radiographs and histologically known patterns of caries. In practice, when a tooth is radiographed and an interproximal region of interest is selected, the software then accesses the database for comparison. The output of the software is in graphical form, which shows whether the area in question is a sound tooth, or a decalcified or carious one. Moreover, the level of false positive or specificity can be adjusted according to the requirement of a clinician [6] [7]. Tracy et al. (2011) studied the performance the of the CAD system where twelve blinded dentists reviewed 17 radiographs [1]. The group concluded that, by using the CAD support, diagnosis of caries increased from 30% to 69%.

Firestone et al. (1998) investigated the effect of a knowledge based decision support system (CariesFinder©, CF) on the diagnostic performance and therapeutic decisions [8]. The study was involved 102 approximal surface radiographic images and 16 general practitioners to identify the presence of caries and whether restoration was required. Their study showed that when the dental practitioners were equipped with a decision support system, their ability to diagnose dental caries correctly, increased significantly.

Similarly, Olsen et al. (2009) proposed a computerized diagnosis system that aimed to give feedback about the presence and extent of caries on the surface of teeth [9]. Their method gave both qualitative and quantitative opinion to dental practitioners, by using digital images and a graphical user interface.

2.2 BONE DENSITY DIAGNOSIS

Kavitha et al. (2012) proposed a CAD system that measures the cortical width of the mandible continuously to identify women with low bone mineral density (BMD) from dental panoramic images [10]. The algorithm was developed using support vector machine classifier where 60 women were used for system training and 40 were used in testing. Results showed that the system is promising for identifying low skeletal BMD. Muramatsu et al. (2013) also proposed a similar work for measuring mandibular cortical width with a 2.8 mm threshold [11]. The algorithm showed 90% sensitivity and 90% specificity.

Reddy et al. (2011) developed a Computer aided diagnostic method to differentiate various metastatic lesions present in the human jawbones from Dental Computed Tomography images [12]. They developed a method to find most discriminative texture features from a region of interest, and compared support vector machine (SVM) and neural network classifier for classification among different bone groups. They have achieved an overall classification accuracy of 95%, and concluded that artificial neural networks and SVM are useful for classification of bone tumors.

2.3 LESION/BONE DEFECT DIAGNOSIS

Shuo Li et al. (2007) developed a semi-automatic lesion detection framework for periapical dental X-rays using level set method [4]. The algorithm was designed to locate two types of lesions: periapical lesion (PL) and bifurcation lesion (BL). Support vector machine was used for segmentation purpose. The algorithm automatically locates PL and BL with a severity level marked on it.

Also Stelt et al. (1991) developed an algorithm to detect periodontal bone defects [13]. They have used image processing techniques to find the lesions that were artificially introduced into the radiographs. Their system was designed to decrease interobserver variability and time-dependent variability.

The work in this research was focused on lesion/bone defect diagnosis on CT images. The proposed method is a fully automatic scheme to highlight any suspicious region regardless the type of a disease. In the following sections, materials used for this work and methodology of the algorithm are discussed, and finally the results are evaluated.

3. MATERIALS

A total oral CT scan of 52 patients were investigated, where 22 patients had abnormalities and 30 patients had normal appearances. Normal and abnormal aspects of these images were verified by a dentist. Each patient had 496 2D axial CT slices. These images were provided by Vatech Co., Ltd, Korea, and were supplied in 16-bit RAW format.

4. METHODOLOGY

This section elaborates the computer aided detection of oral lesions in mandibular region (Figure 4.2). The framework consists of two algorithms for detection of two types of lesions: Closed boundary lesions (Type I) and Bone deformation (Type II) (Figure 4.1). This classification is not done on a medical basis, and is used for research purpose only. In addition, the goal of this CAD scheme was not to detect a specific syndrome, rather any kind of abnormality regardless of the diseases type. Therefore, the classification of lesions considered here served as a generalized grouping of all type of abnormalities that could be found in dental CT images. To define, a closed boundary lesion is one that has a well-defined boundary around the lesion, and a bone deformation problem is one that has a broken boundary line around the lesion. Methods for detecting these two types of lesions are described in the later sections.

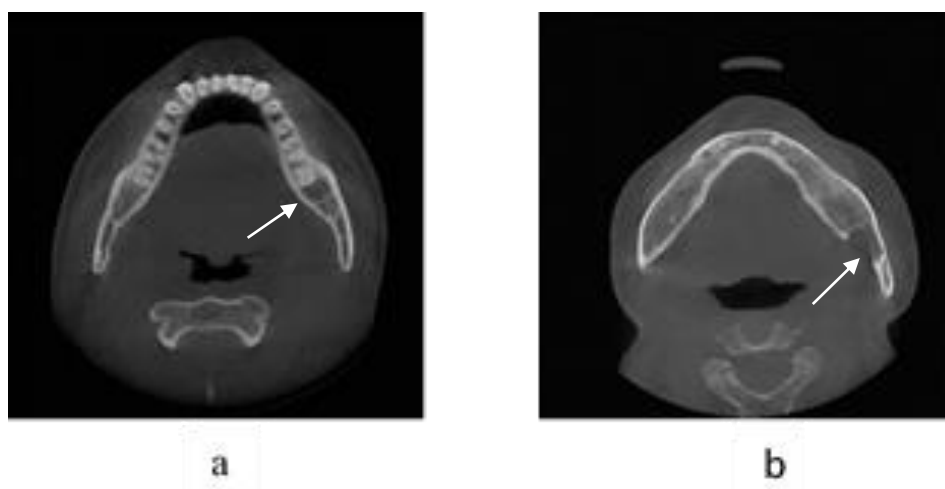


Figure 4.1. Illustration of two types of Lesions. (a) Closed boundary lesion, (b) Bone deformation lesion

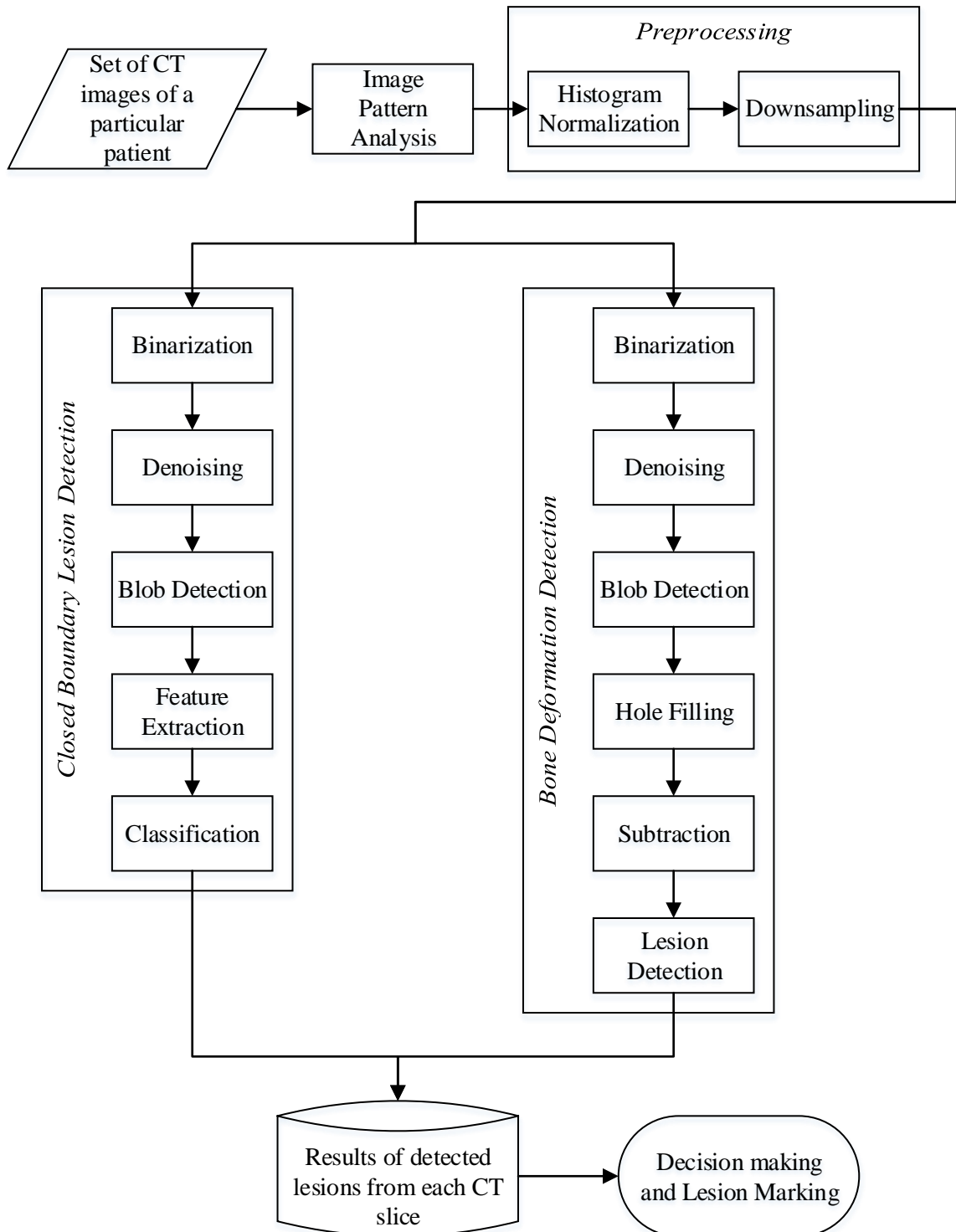


Figure 4.2. Architecture of the proposed method

4.1 IMAGE PATTERN ANALYSIS

Every CT scan of a particular patient had nearly 500 CT slices for the cases considered (Figure 4.4). Each slice represents different cross-sectional view of different parts of oral anatomy. Therefore to check the various abnormalities in different oral anatomy, an approximate estimation of image pattern was needed. To estimate the pattern mathematically, three histogram based parameters such as standard deviation, skewness and kurtosis were calculated for every CT slice of a particular patient. Among these parameters, kurtosis values were found promising to assess image pattern. When kurtosis value of the slices were plotted against the slice number; Figures similar to Figure 4.3 were obtained for different patients. From the observation of actual images, it was concluded that, the peak “A” in the mid-section of Figure 4.3 approximately separates the maxilla and mandible region (Figure 4.4). The assumption was made based on the statistics of 22 abnormal and 30 normal patient cases. From the slice number of peak “A”, next slices were considered for finding abnormality in the mandibular region.

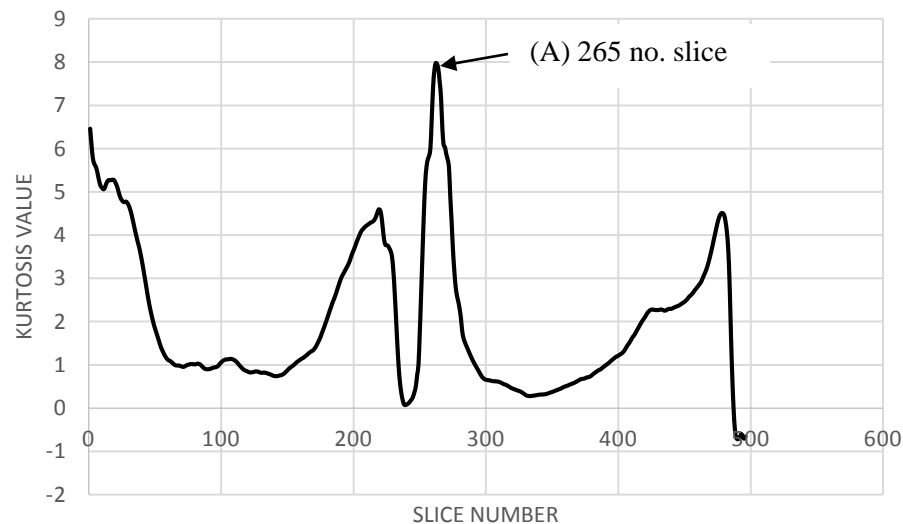


Figure 4.3. An example plot of image pattern analysis

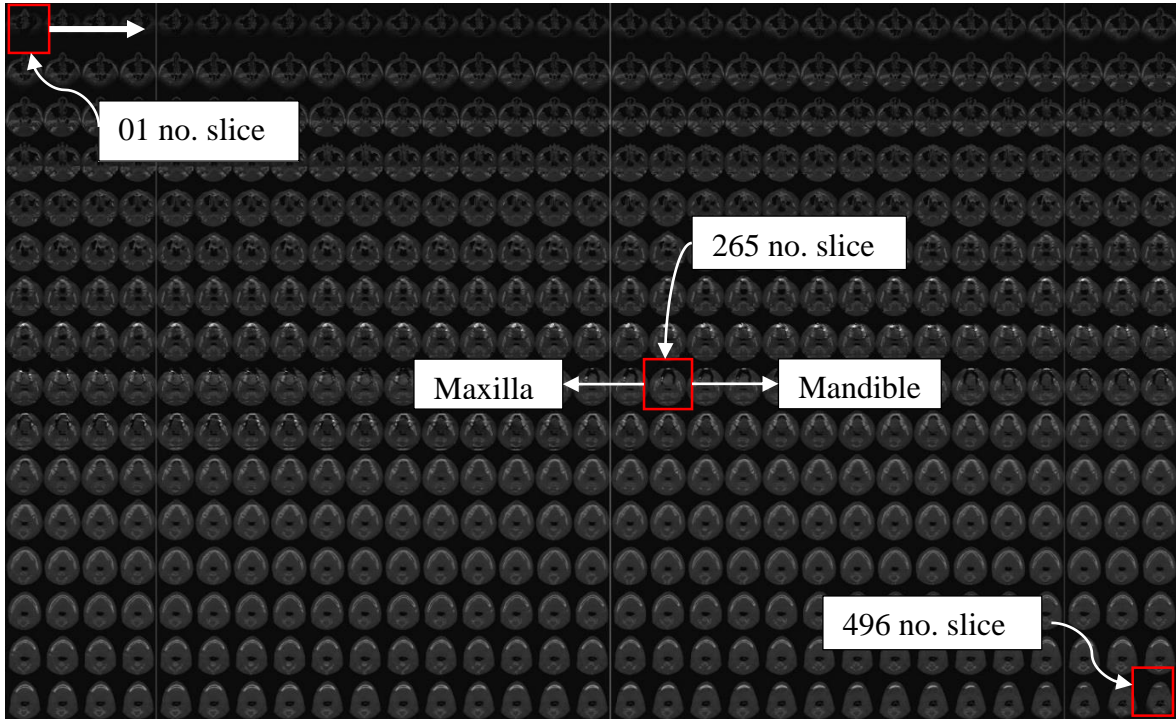


Figure 4.4. Illustration of all the CT slices (496) for a single patient. The red box in the middle indicates the image that roughly differentiates between maxilla and mandible.

4.2 PREPROCESSING

Image preprocessing was required for reducing contrast variation among different images (Figure 4.5). Contrast variation occurs due to use of different scanners and also for different dose rate. Enhancing contrast of the image also improves the possibility of manipulation of the dataset. Therefore histogram normalization was carried out for enhancing the contrast of the image using Formula 1. Moreover, image data was converted from 16-bit signed integer to 8-bit unsigned integer to reduce the computational cost (Figure 4.5 (b)). Furthermore, image was subsampled to half size (400x400 pixels) (Figure 4.5 (c)) for additional reduction of the computational time.

$$I_{out(x,y)} = 255 \left(\frac{I_{in(x,y)} - I_{in,min}}{I_{in,max} - I_{in,min}} \right) \quad (1)$$

Where $I_{out(x,y)}$ is the output gray level intensity at (x, y) coordinate.

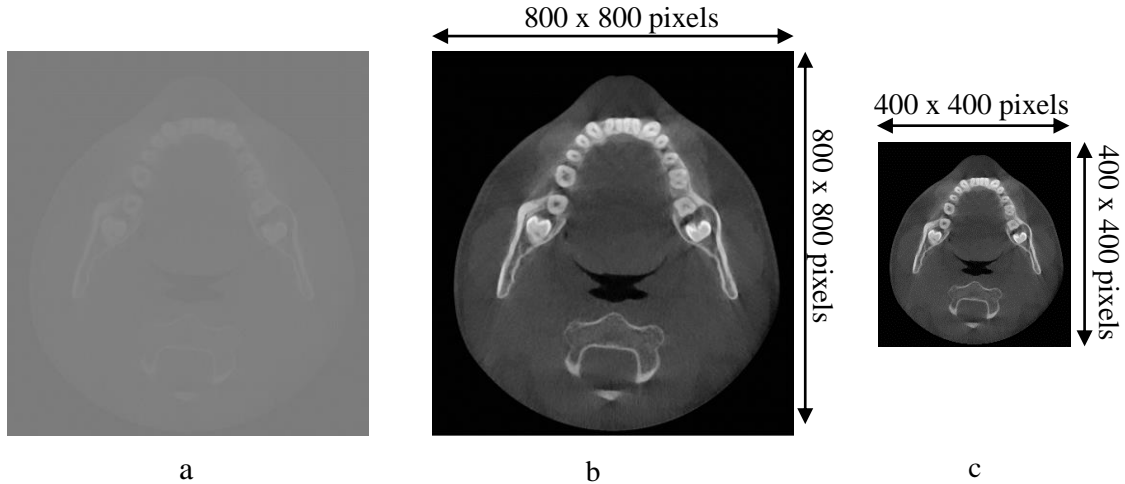


Figure 4.5. Illustration of preprocessing process. (a) 16-bit raw image (b) 8-bit histogram normalized image (c) Subsampled image

4.3 DETECTION OF CLOSED BOUNDARY LESION (CBL) (TYPE I)

A closed boundary lesion in dental CT images was assumed as a low intensity region surrounded by a relatively high intensity boundary around it. These regions can be circular, elliptical or any irregular shape. The problematic regions were usually neither very large nor very small in size, and had unique texture and statistical properties. These regions were visually homogenous and could be identified in several slices for a particular patient. These were the main assumptions about a lesion for designing closed boundary lesion detection algorithm.

CBL detection algorithm was designed in three stages: initial lesion candidate detection, feature extraction and classification (Figure 4.6). These stages are described in sequential sections.

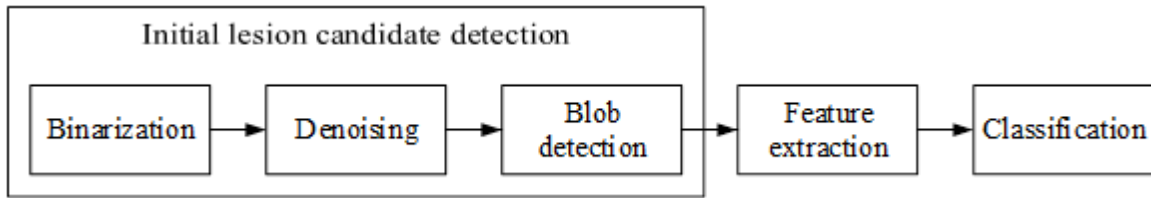


Figure 4.6. Block diagram of Closed boundary lesion detection method

4.3.1. Initial Lesion Candidates Detection. The purpose of initial lesion candidate detection is to detect all the possible areas that could be a potential lesion. Potential CBLs can be viewed as blobs in a digital CT image. ‘Blob’ can be understood as ‘regions’ in images that differ in properties compared to its surrounding area. Therefore blobs are different areas in an image, similar in properties among themselves but different from the background. Furthermore, detecting blobs simplifies the algorithm process greatly as then only the detected blobs need further inspection instead of the full image. Sensitivity of this blob detection process was high so the chances of missing out a possible lesion candidate was low in this stage.

4.3.1.1. Binarization. At first, binary image was computed from original gray scale image using ‘Maximum Entropy threshold’ method [14], which is an automatic threshold process. Image processing with binary images had several advantages, such as easier processing and analyzing data with minimum loss of information. Calculating appropriate threshold value for binarization was vital for the performance of detection because inaccurate threshold could eliminate possible lesion candidates. This specific method was chosen from experimental observations of a few already developed automatic threshold methods. Results of some automatic threshold methods are shown in Figure 4.7. The methods studied are: Li’s method [15], Kapur-Sahoo-Wong method [14], Mean method [16], Kittler and Illingworth’s Minimum Error thresholding method [17], Prewitt and Mendelsohn’s method [18], Tsai’s method [19], Otsu’s method [20], Doyle’s method [21], Renyi’s entropy method [14], Shanbhag and Abhijit’s method [22], Triangle method [23] and Yen’s method [24].

From Figure 4.7, it can be seen that Kapur-Sahoo-Wong's Maximum Entropy method (Figure 4.7 (b-2)), Renyi's entropy method (Figure 4.7 (b-9)), and Yen's method (Figure 4.7 (b-12)) could be the possible choices for binarization. Among these options, Kapur-Sahoo-Wong's Maximum Entropy method was selected for the algorithm due to its simplicity of implementation. In Maximum Entropy method, two probability distributions were derived from the original gray level image; one was for object distribution and other was for background distribution [25]. The distributions were expressed as:

$$\frac{p_0}{P_t}, \frac{p_1}{P_t}, \frac{p_2}{P_t}, \dots, \frac{p_t}{P_t}$$

and

$$\frac{p_{t+1}}{1 - P_t}, \frac{p_{t+2}}{1 - P_t}, \frac{p_{t+3}}{1 - P_t}, \dots, \frac{p_{l-1}}{1 - P_t}$$

Where t is the value of the threshold and $P_t = \sum_{i=0}^t p_i$. Then define,

$$H_b(t) = - \sum_{i=0}^t \frac{p_i}{P_t} \log_e \left(\frac{p_i}{P_t} \right)$$

$$H_b(t) = - \sum_{i=t+1}^{l-1} \frac{p_i}{1 - P_t} \log_e \left(\frac{p_i}{1 - P_t} \right)$$

Then the optimal threshold t^* is defined as the threshold which maximizes $H_b(t) + H_w(t)$.

$$t^* = \underset{t \in G}{\text{ArgMax}} \{H_b(t) + H_w(t)\}$$

Where $G = \{0, 1, 2 \dots l-1\}$ is the set of positive integers representing gray levels.

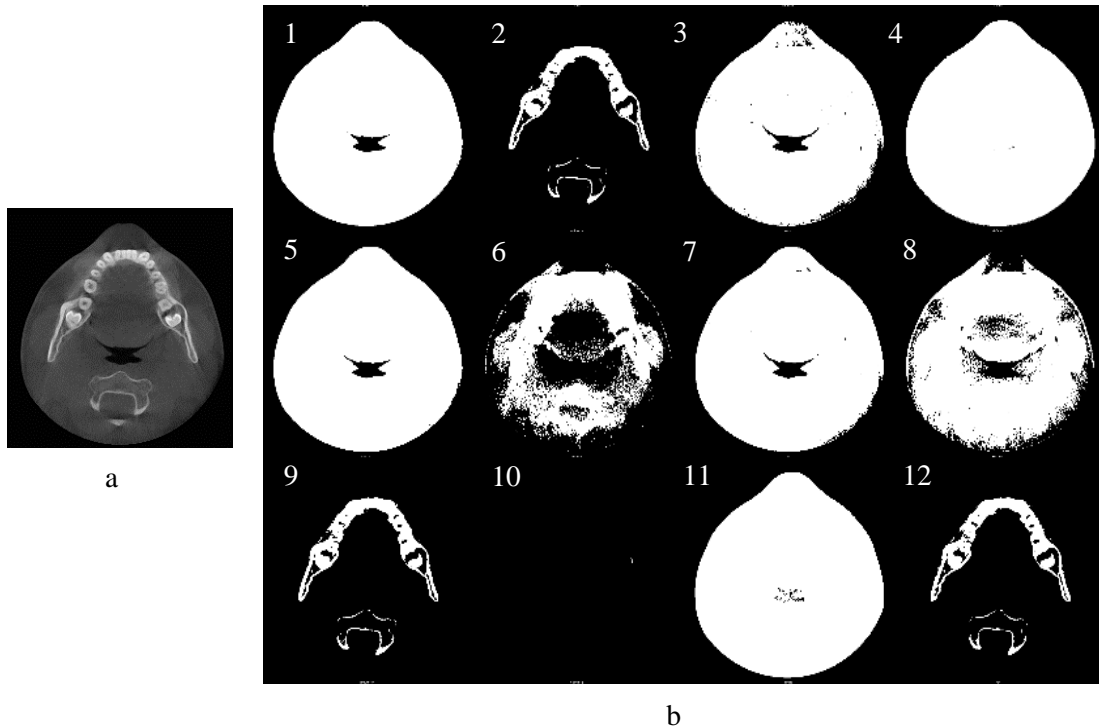


Figure 4.7. Example of some automatic threshold methods. (a) Intensity image, (b) Binary image calculated in different methods: (1) Li's method, (2) Kapur-Sahoo-Wong method, (3) Mean method, (4) Kittler and Illingworth's Minimum Error thresholding method, (5) Prewitt and Mendelsohn's method, (6) Tsai's method, (7) Otsu's method, (8) Doyle's method, (9) Renyi's entropy method, (10) Shanbhag and Abhijit's method, (11) Triangle method, (12) Yen's method

4.3.1.2. Denoising. After computing the binary image, morphological closing operation [26] was carried out to eliminate some noises from the binary image (Figure 4.8). Morphological operations were very useful techniques to remove imperfections by accounting for architecture of the image. Figure 4.8 (b) shows the filtered image where most of the noises were removed from the binary image. Structuring element for this operation was chosen in such a way that it would fill holes of size up to 5mm. Holes larger than 5mm were considered as a possible lesion.



Figure 4.8. Illustration of denoising process. (a) Binary image (noise present), (b) Denoised image after morphological filtering.

4.3.1.3. Blob detection. Finally, all possible lesion candidates were filtered out from denoised image by implementing blob detection [27] method which was developed by Haralick et al. (1992). All blobs larger than 5mm in size were detected by “Connected component labelling” algorithm [27]. After detection, only the blobs that were above 1/3 height from the bottom of the image, were selected for further processing (Figure 4.9 (a)), because the anatomy present in the bottom 1/3 of the image area, was less likely to represent a lesion. Figure 4.9 (b) shows the detected blobs (total: 4) from the filtered image. These blobs represented initial lesion candidates.

4.3.2. Feature Extraction. The purpose of feature extraction is to acquire sufficient information about an image area, to be classified into different categories. Features are computed from image intensity values. Features, also known as feature vectors, were calculated for each initial lesion candidate detected. Once all the initial lesion candidates were detected, bounding rectangle around each blob were calculated (Figure 4.10 (a)). The rectangles were then superimposed over the intensity image in the same position relative to the detected blobs (Figure 4.10 (b)). Then image section inside each rectangle were cropped out for feature extraction and these image sections were considered as “Region of Interest” or “ROI”.

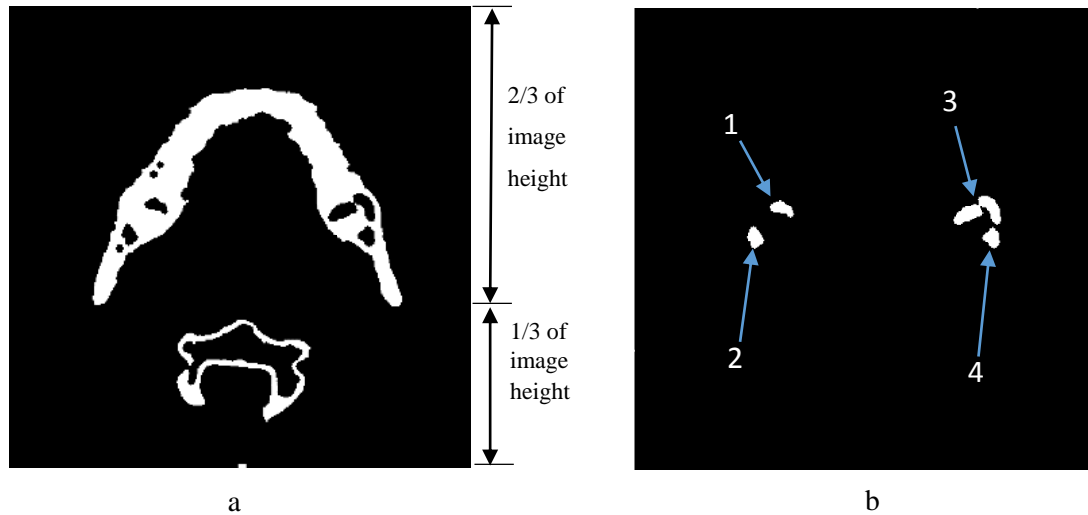


Figure 4.9. Illustration of blob detection process. (a) Filtered image, (b) Detected blobs from filtered image (4 blobs were detected)

Three types of features were extracted from each ROI. These features were commonly known as First order statistics, Second order statistics and Image moments. A short description of these features are described as follows:

4.3.2.1. First order statistics. First Order Statistics are the standard statistical measures of gray level values of a ROI, such as mean, standard deviation, skewness and kurtosis. These statistics are calculated from gray level intensity values of the ROI. The feature set is widely used in image processing and is a basic feature set. First order statistics alone often cannot distinguish between different image textures.

4.3.2.2. Second order statistics. Second order statistics, calculated from Grey-Level Co-occurrence Matrices (GLCM) [28], are a good measure of image texture. This feature set was developed by Haralick et al. (1973) and was used in many real world applications for its reasonable performance in discriminating different image textures. Four second order statistics features were calculated in this algorithm namely: contrast, homogeneity, energy and entropy. For the computation of GLCM, only horizontal position of neighboring pixels were considered. A short description of these features are described below:

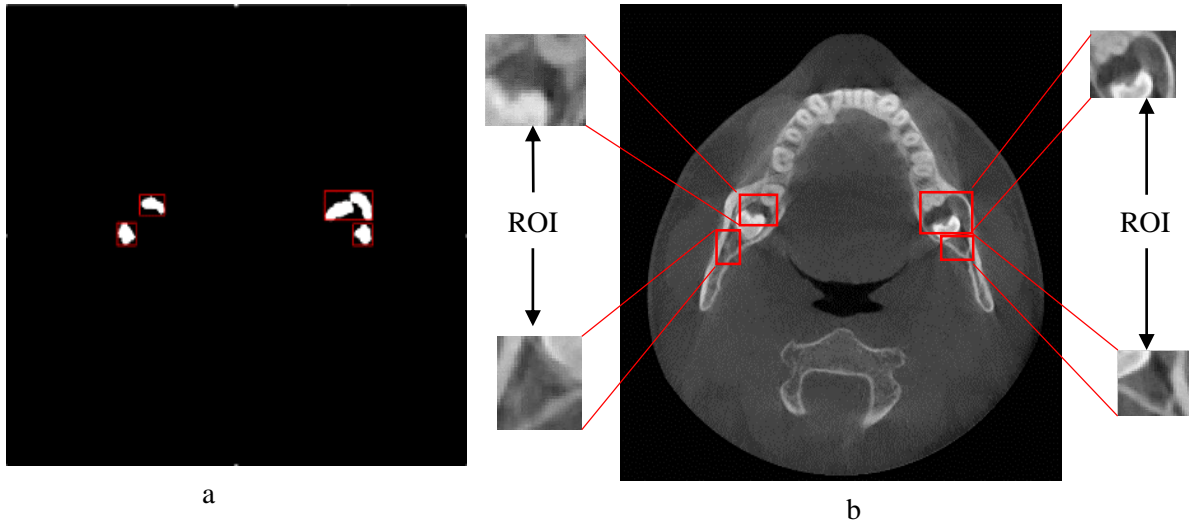


Figure 4.10. Illustration of ROI extraction process. (a) Bounding rectangles calculated around each blob, (b) Bounding rectangles were superimposed over the intensity image and ROIs were cropped out.

Contrast is the gray level variation of the co-occurrence matrix. It computes a linear relation of gray levels between neighboring pixels and describes amount of local variations present in an image [28]. Therefore higher local variation will yield higher contrast value and vice versa. Contrast is calculated by equation 2:

$$Contrast = \sum_{i,j} |i - j|^2 p(i, j) \quad (2)$$

where $p(i, j)$ stands for $(i, j)^{th}$ value in a normalized GLCM, which is true for all GLCM formulas.

Homogeneity is the measure of uniformity of non-zero pixels in an image [29]. If the image has little variation then the homogeneity is high and if there is large variation then the value is low. An inhomogeneous image is one where there is no special similarity is present [30].

$$Homogeneity = \sum_{i,j} \frac{1}{1 + (i - j)^2} p(i, j) \quad (3)$$

Entropy represents the spatial disorder of gray level values. A random texture would have a very high entropy value whereas a solid texture would have a very low value. This feature can describe the difference between heavy texture and smooth texture and can also indicate if there is a pattern present or not [30].

$$Entropy = -\sum_{i,j} p(i,j) \log(p(i,j)) \quad (4)$$

Energy represents the opposite of entropy. It tells about the uniformity or randomness of the texture calculated in a different way. The higher the energy value, the more uniform the texture in that image[30].

$$Energy = \sum_{i,j} p(i,j)^2 \quad (5)$$

4.3.2.3. Image moments. Image moments provide a special kind of weighted average of image pixels' intensities. Moments usually provide attractive information such as geometry information of objects in an image. Hu (1962) [31] developed seven image moments which are independent of position, size, orientation and parallel projection. Among seven moments, six are absolute orthogonal invariants and the other one is skew orthogonal invariant based upon algebraic invariants. Image moments have been widely used in pattern recognition, image registration and pattern recognition [32]. However, Hu's moment invariants fluctuate in different scale and rotation of the image [32]. But the changes are not remarkable when image resolution is decent. Therefore, Hu moments are expected to offer close values for similar patterns when the image resolution is high. Seven Hu moment features were calculated for extracting geometry information from ROI.

Therefore, total fifteen (First order statistics: 4, Second order statistics: 4, moments: 7) feature vectors were calculated to classify a region as normal or abnormal.

4.3.3. Classification. Purpose of classification is to classify data into different classes such as normal and abnormal. Fifteen feature vectors were used to classify a region in this algorithm.

Artificial Neural Network (ANN) is one of the few machine learning classifiers that is used for classifying data which are not linearly separable. ANN also showed excellent results in several medical image analysis applications [33]. In this method, Multilayer Perceptron (MLP) neural network was used for classifying data between two groups i.e. Lesion and Normal. ANN is a supervised classifier, which learns from examples of known normal and abnormal samples.

A multilayer perceptron (MLP) is a feedforward artificial neural network model. It maps sets of input data onto a set of appropriate outputs. It is a network of simple neurons called perceptron. The basic idea of a single perceptron was introduced by Rosenblatt in 1961 [34]. In a MLP, multiple layers of nodes are present, where each layer is fully connected to the next one. Except for the input nodes, each node has a nonlinear activation function. This MLP uses a learning technique called backpropagation for training the network, which is a supervised method. The example in Figure 4.11 represents a 3-layer perceptron with four inputs, two outputs, and the hidden layer including four neurons

All the neurons in MLP are alike. Each of them takes the output values from several neurons from the previous layer as input and passes the response to several neurons in the next layer. The values retrieved from the previous layer are summed up with certain weights, distinct for each neuron and the bias term is added. The activation function φ then transforms the sums which may be also different for different neurons. Mathematically, output from a neuron:

$$y = \varphi(\sum_{i=1}^n w_i x_i + b) \quad (6)$$

Here w denotes the vector of weights, x is the vector of inputs, b is the bias and φ is the activation function. A signal-flow graph of this operation is shown in Figure 4.12.

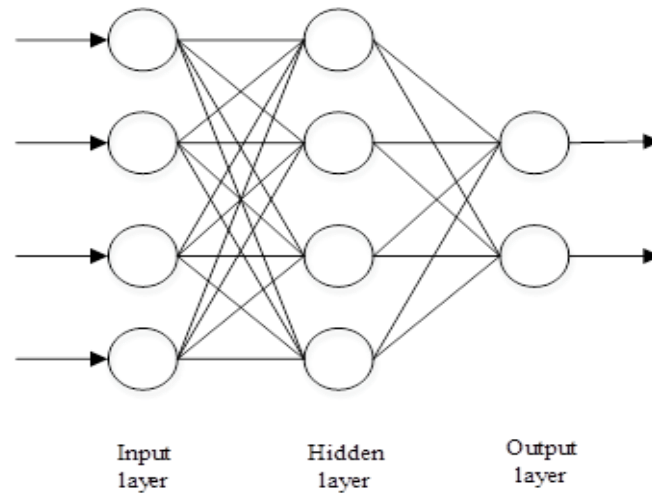


Figure 4.11. Configuration of multi layer perceptron neural network

The two leading activation functions used in current applications are both sigmoids, and are described by,

$$y_i = \varphi(u_i) = \tanh(u_i) \text{ or } \varphi(u_i) = (1 + e^{-u_i})^{-1} \quad (7)$$

$$\text{where, } u_i = \sum_{i=1}^n w_i x_i + b$$

The former function (φ) is a hyperbolic tangent. It ranges from -1 to 1. And the latter is the logistic function, ranges from 0 to 1. In equation 7, y_i is the output of the i^{th} node and u_i is the weighted sum of the input synapses.

Therefore the network takes feature vectors as inputs where size of input layer is equal to the number of feature vectors, forwards the values to the next hidden layer and computes outputs using weights and activation functions and passes the outputs to further downstream until the computation of output layer.

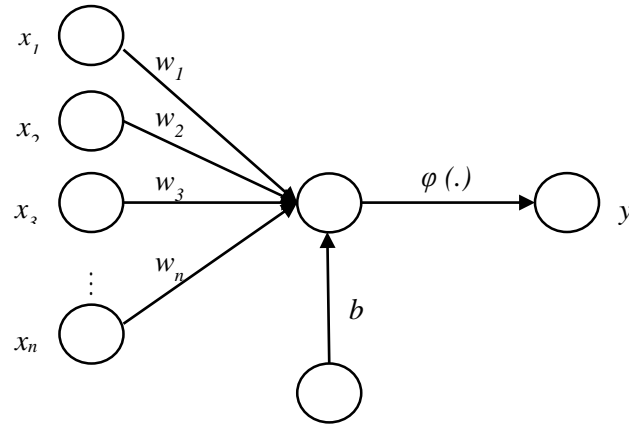


Figure 4.12. Flow diagram of a single neuron

MLP neural network is trained with backpropagation learning [35]. Sample ROIs are used to train the neural network, where both normal and abnormal examples are present. (Figure 4.13). Data from ROIs are collected manually and by using blob detection and feature extraction algorithms. The neural network has a configuration of fifteen (15) input layer nodes for fifteen (15) feature vectors, ten (10) hidden layer nodes, and two (2) output layer nodes. Figure 4.14 shows the schematic diagram of the training process.

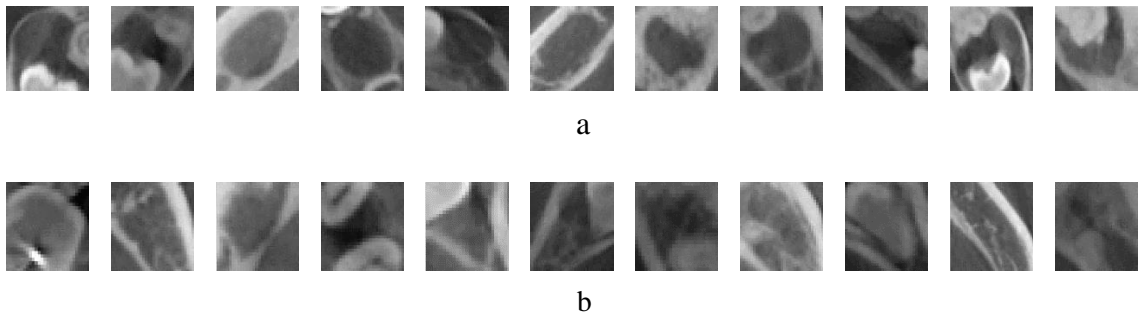


Figure 4.13. Illustrations of training samples (a) Samples of lesion ROI, (b) Samples of normal ROI

Once the neural network training has been completed and all of its weights are adjusted to the optimum configuration, the network is used for unseen data classification.

Fifteen feature vectors were calculated from each cropped section and the data was then supplied as input for the trained neural network. Neural network then classified the data between lesion and normal class. If the ROI was found as a lesion class, it was considered as a probable lesion case and its Cartesian coordinate position was calculated for further decision making (Figure 4.15).

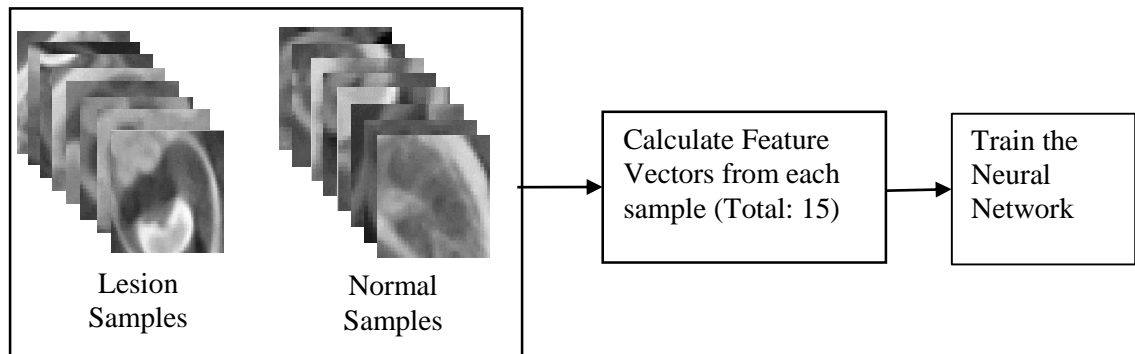


Figure 4.14. Training of Artificial neural network

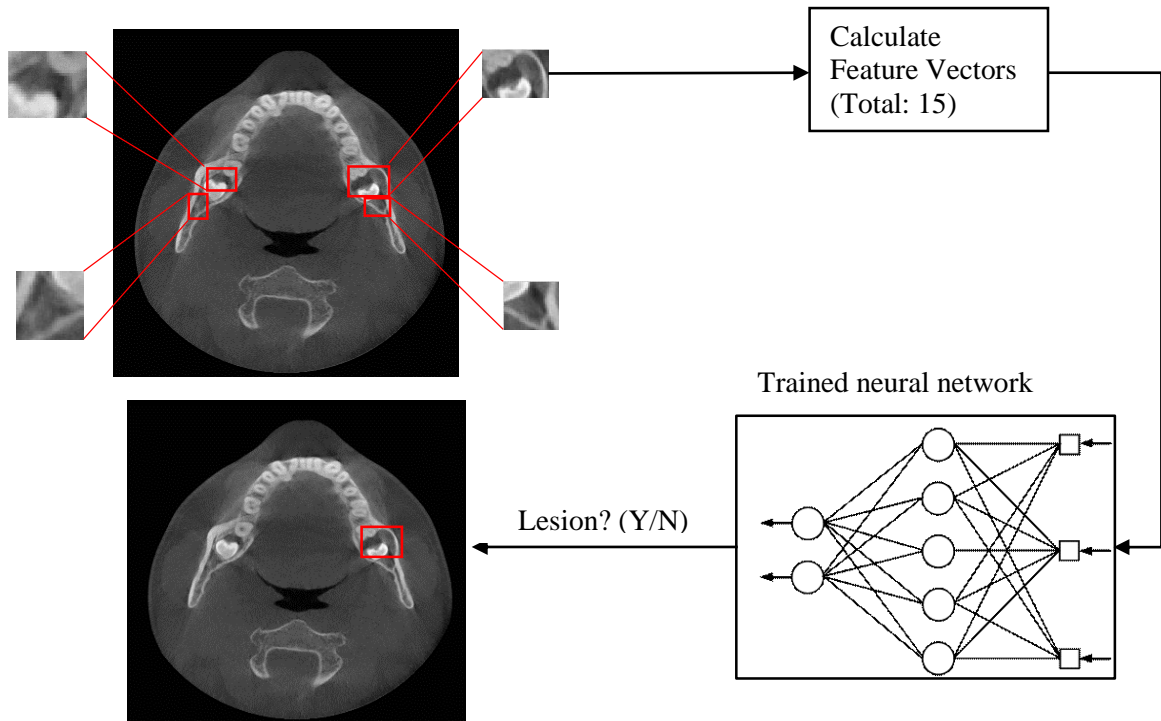


Figure 4.15. Illustration of classification process by neural network

4.4. DETECTION OF BONE DEFORMATION (TYPE II)

Bone deformation problems cannot be solved by blob detection method as lesions had no distinctive close border separating it from background. However, this problem was solved by using morphological image processing operations. At first, binary image was calculated from intensity image by maximum entropy threshold method discussed in the Binarization section. Then the binary image was filtered two times by morphological closing operation with different structuring elements each time. Finally the filtered images were subtracted to get the location and size of the deformed area. The method is described according to Figure 4.16:

- Step 1. In the first stage, image processing described in the “Preprocessing” section was carried out. A 2D RAW slice image was converted to 8-bit gray level image and subsampled to 400x400 pixels (Figure 4.16 (1)).

- Step 2. The intensity image was then transformed to binary image using Kapur's maximum entropy method which was discussed in the "Binarization" section (Figure 4.16 (2)).
- Step 3. Morphological closing operation was carried out on the binary image according to the description in the "Denoising" section. Structuring element for this closing operation was designed to remove noise (small holes or openings) and artifacts from the binary image (i.e. closing with small disk shaped structuring element). Holes or openings smaller than 5mm diameter were considered as noise. Moreover, any anatomy present in the bottom 1/3 of the image was eliminated by using blob detection method discussed in the "Blob detection" section. The anatomy was not considered for further calculation because this part is not expected to represent any lesion (Figure 4.16 (3)).
- Step 4. Again morphological closing operation was carried out to fill large sized holes or openings (i.e. closing with bigger disk shaped structuring element) in the denoised image. The design of the structuring element was such that it can fill holes between 5mm to 30mm of diameter (Figure 4.16 (4)).
- Step 5. Output image from step 3 was then subtracted from image of step 4. The resulting image will contain any architectural defect present in the intensity image. In this stage, blob detection algorithm was carried out again to find any blob that is larger than 5mm diameter and smaller than 30mm diameter. If any blob found within the specified range, then it was considered as a lesion (Figure 4.16 (5)).
- Step 6. Finally the detected blob centroid was calculated and considered as a probable lesion position (Figure 4.16 (6)).

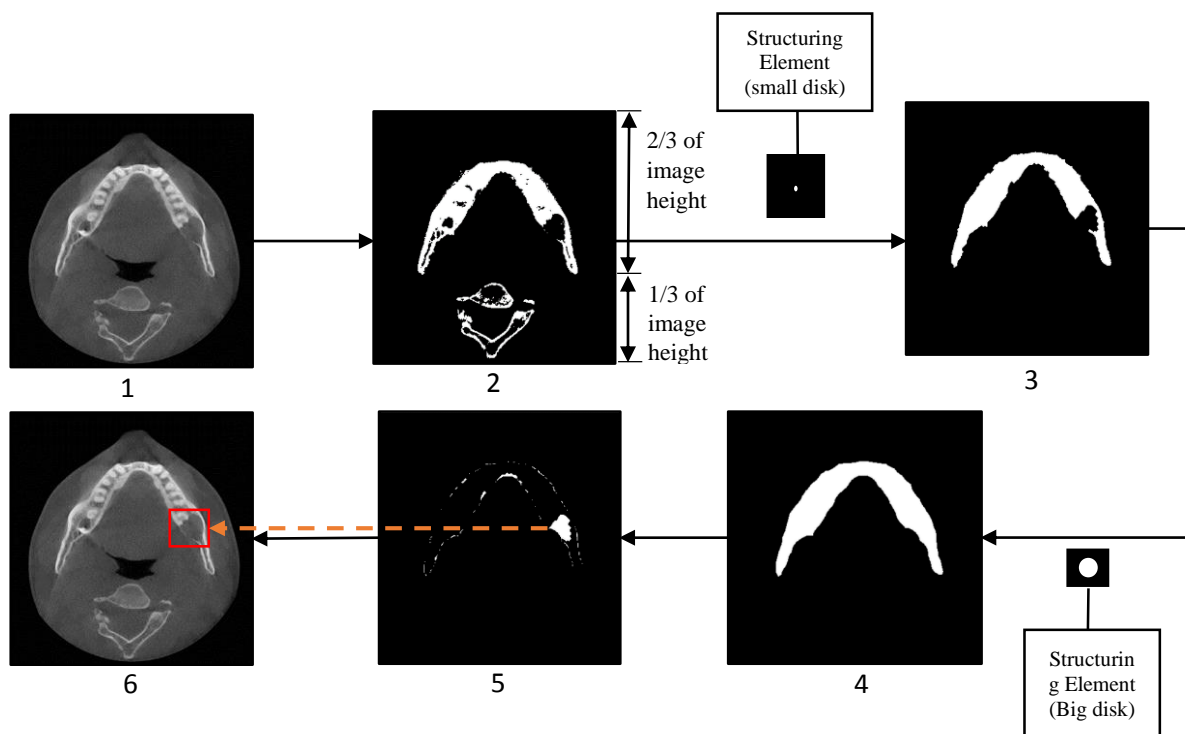


Figure 4.16. Illustration of Bone deformation lesion detection process. (1) Pre-processed intensity Image, (2) binary image, (3) Noise reduction by morphological closing operation and blob detection above 1/3 height from the image bottom, (4) Large hole filling by morphological closing operation with a larger structuring element on the denoised image, (5) Subtraction result of image 3 from image 4. Then blob detection carried out to find any architectural defect, (6) Detected area marked on the intensity

4.5. DECISION MAKING AND LESION AREA MARKING

Final decision for a lesion was only made if same lesion position was detected in at least five consecutive CT slices. An actual lesion is expected to have appearances in multiple CT slices. This rule of thumb was used to eliminate many false positives that were detected randomly. Finally the detected area was marked for further diagnosis of a dentist.

5. RESULTS AND DISCUSSIONS

In this section, results of the two algorithms are discussed separately. In the first section, results of closed boundary lesion detection algorithm have been evaluated, and results of bone deformation detection algorithm will be evaluated in the later section.

In our CT dataset, 22 patients contained oral lesions where 14 (10+4) patients had closed boundary lesions and 12 (8+4) patients had bone deformation lesions (Figure 5.1). For 4 of the patients, both types of problems were identified. We had also included 30 patients who did not have any lesions (normal cases). Thus, 52 CT cases compose the dataset to evaluate the lesion detection framework.

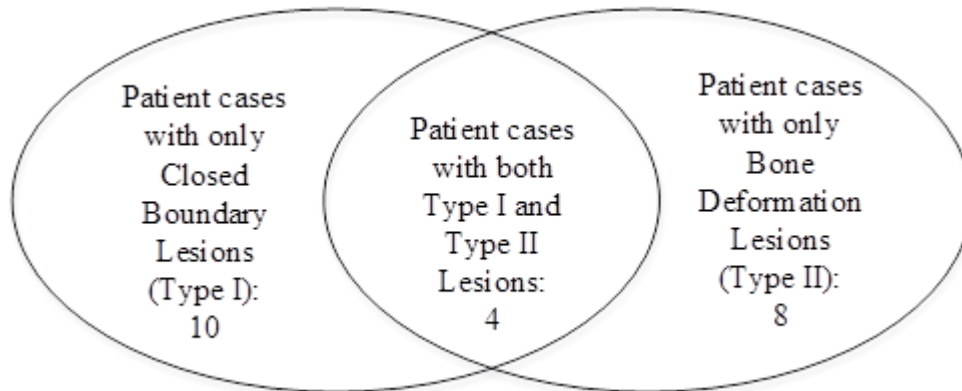


Figure 5.1. Distribution of abnormal patient case dataset

Free Response Receiver Operating Characteristics (FROC) curves were used for evaluating the CAD system. Sensitivity and false positive per patient were the parameters used for FROC curves where,

$$\text{Sensitivity} = \frac{\text{True Positive cases}}{\text{True Positive cases} + \text{False Negative cases}}$$

$$\text{False positive per patient} = \frac{\text{False Positive cases}}{\text{False Positive cases} + \text{True Negative cases}}$$

We have considered a patient as true positive if the detected lesion was marked inside of it. False negative patients were those who had lesions but the algorithm didn't detect any abnormality. A case was considered as false positive if a healthy region was detected by the algorithm. And a case was true negative if a normal patient was identified as normal.

5.1. EVALUATION OF CLOSED BOUNDARY LESION DETECTION ALGORITHM.

To validate the proposed closed boundary lesion detection algorithm, we divided the closed boundary patient cases into two sets- one for training purpose and the other for testing purpose. Training set contained 7 abnormal and 15 normal patient cases and testing set contained 7 abnormal and 15 normal patient cases, which made the validation dataset. We selected our training set in a manner that patients with similar lesions contained in the training set as less as possible. Therefore, our training set had large variance and bias which made it tougher for neural network to generalize the output.

Results of the algorithm is presented in Figure 5.2. The testing set yielded about maximum 71% sensitivity with 0.31 false positives per patient. The FROC curve shows results at different operating points where the algorithm can be functioned. The method achieved minimum 0.12 false positives per patient with 33% sensitivity. However, when all the 14 closed boundary patient cases and all 30 normal patient cases were used for training, and the same dataset was used for testing, maximum 92% sensitivity was achieved with 0.32 false positives per patient. The algorithm also showed about 80% sensitivity at 0.03 false positives per patient.

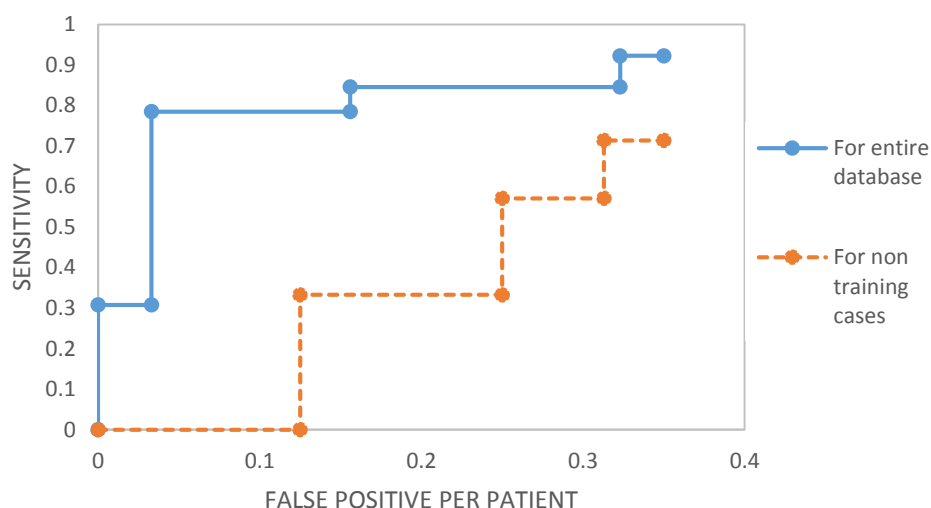


Figure 5.2. Comparison of FROC curves in closed boundary lesion detection. The solid curve indicates the results of the scheme when entire closed boundary dataset was used for both training and testing (14 abnormal and 30 normal patients). The dotted curve indicates the results when testing set was not used for training.

The major limitation of the algorithm was that it was not designed to detect any lesion that is brighter than its surroundings. It was an initial assumption that the lesions are darker than its surroundings. Image processing involved here accommodates to find initial lesion candidates inside mandibular bone that has less intensity than its neighboring area. Therefore to detect brighter lesions, a new algorithm could be developed which was not studied in this research.

Moreover, the algorithm performance was lower for the lesions that does not have a well-defined boundary around it. Sometimes these lesions are very difficult to identify because they are very similar to the image background noise and therefore rejected by the algorithm as false positives. These type of cases were usually considered as “difficult to identify” cases in medical image interpretation algorithms.

Lesion size also had an impact to the performance of the algorithm. Our method intends to achieve high detection accuracy on oral lesions sized between 7.5mm to 20mm

diameter. Detection accuracy decreased for lesions larger than 25mm or smaller than 7mm diameter.

Performance of a method where neural network is used for classification or pattern recognition purpose, depends on the sufficient availability of example data for training. Closed boundary lesion detection method had used only 7 normal and 15 normal example cases which was a very small amount for training a neural network. However, still the algorithm performed in an acceptable manner by indicating 71% sensitivity. Upon availability of additional example cases, the algorithm is expected to predict results with better accuracy and could be used in clinical context.

5.2. EVALUATION OF BONE DEFORMATION DETECTION ALGORITHM

The bone deformation algorithm yielded better results than the closed boundary algorithm. It achieved 85% sensitivity without any false positives on the bone deformation dataset of 12 abnormal and 30 normal patients. Moreover, the algorithm was able to achieve 100% sensitivity with just 0.13 false positives per patient (Figure 5.3).

However, the algorithm was able to detect lesions of diameter between approximately 10mm – 25mm without compromising its accuracy greatly. If any lesion has larger or smaller size than the indicated value, then the system performs at a reduced accuracy rate due to its unique image processing procedure. The image processing involved morphological operations, which required to prespecify the structuring element size. As the structuring element size was an empirical constant for the algorithm, modifying the size limitation increased the false positive rate. The structuring element size was adapted from the example lesions. If necessary, the element size can be further adjusted to identify small or oversized lesions.

In the bone deformation algorithm, no feature extraction or classification method was used. It was a rule based algorithm. Therefore there was no need to validate the algorithm by dividing the dataset into training and testing cases. The algorithm was validated by dentist's decision about healthy or lesion regions. Figure 5.3. Shows the performance of the algorithm at different operating points.

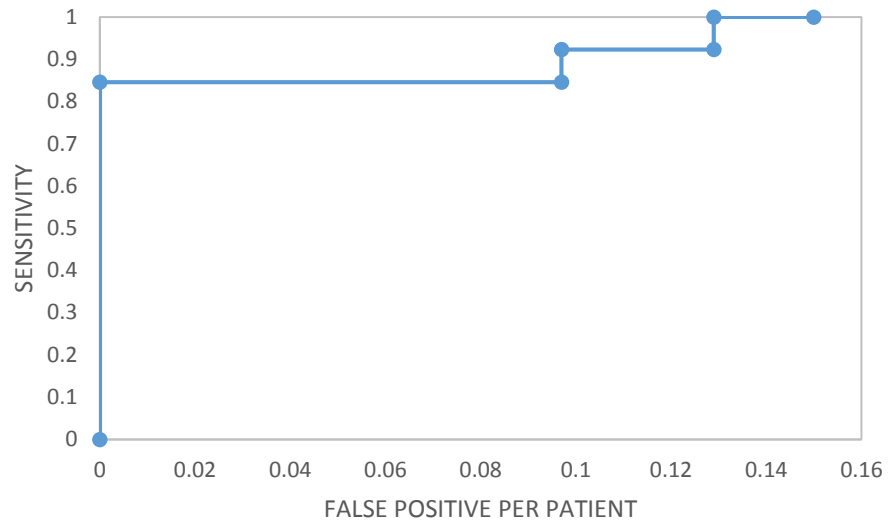


Figure 5.3. FROC Curve of Bone deformation detection algorithm

Both of the algorithms were implemented on C++ language. It took 7 – 10 seconds for executing the algorithms together for a single patient. Computer used for the testing had core i7, 4.00 GHz processor with 16 GB of RAM.

6. CONCLUSIONS

An approach to detect oral lesions in mandible region on CT images have been proposed in this work. Two types of lesions namely closed boundary lesion and bone deformation lesion were identified which covered most of the problems that could be found on oral CT images. Results suggest that the method is capable to detect closed boundary lesions with 71% sensitivity at 0.31 false positives per patient and bone deformation lesions with 100% sensitivity at 0.13 false positives per patient.

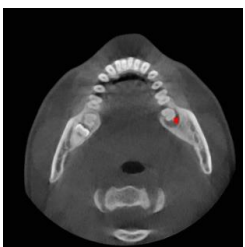
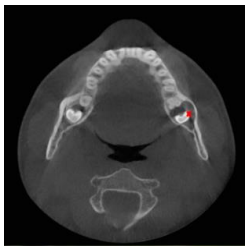
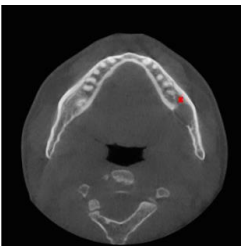
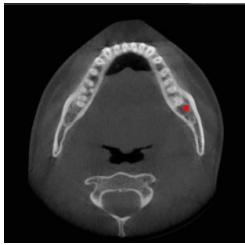

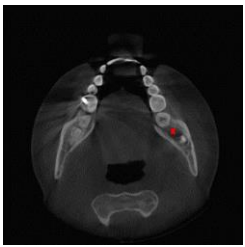
Some of the limitations of the algorithm includes: it cannot detect lesions brighter than its surroundings, lack of a well-defined boundary around a lesion decreases the detection accuracy and too large or too small lesions achieved less detection sensitivity. However, availability of more example images are expected to improve the results and overcome the limitations.

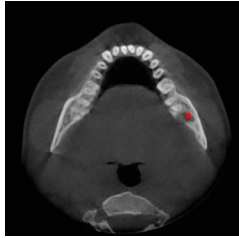
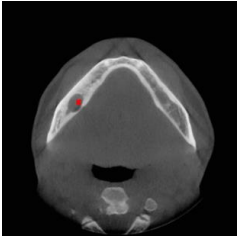
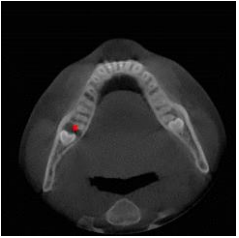
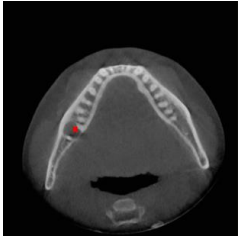
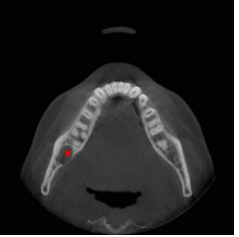
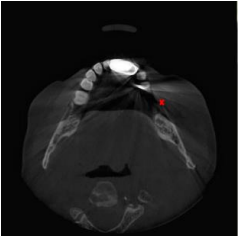
The work done in this research focused on the mandibular region of the oral anatomy. Therefore, future research possibilities in this CAD framework includes: detection of lesions in maxilla, detection of brighter lesions and improve the detection accuracy for lesions with unclear appearances.

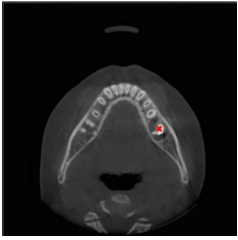
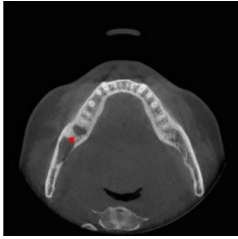
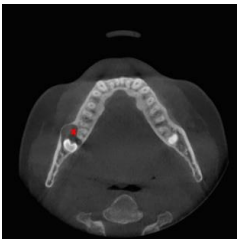
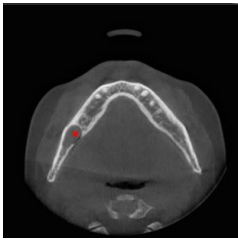
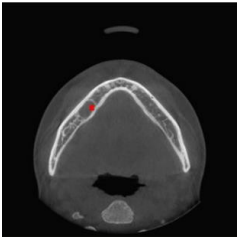
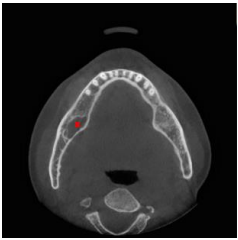
APPENDIX


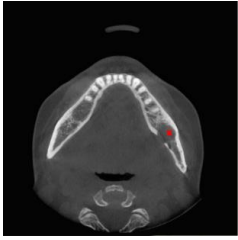
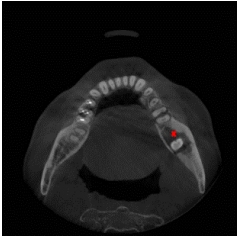
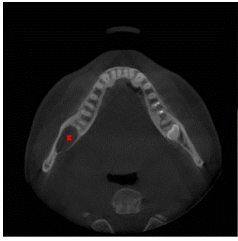

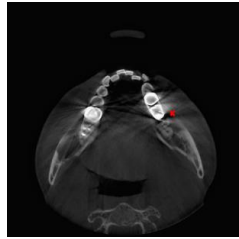
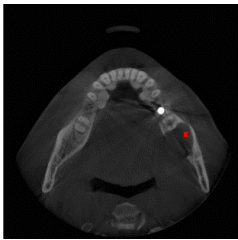
This section contains the output images of the proposed method. We have only included images of 22 patients who had abnormalities. For some patients, lesion was detected by both of the algorithms (i.e. Patient case no. 2, 7, 12 and 15). These results were obtained by setting the operating threshold of the algorithm at a point where false positive rate was minimum at a practical sensitivity.

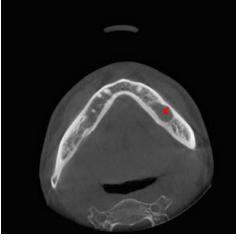
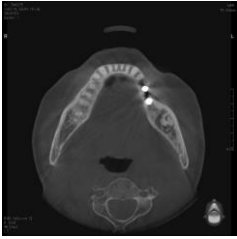
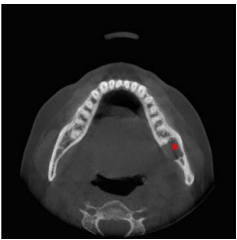
Table. Results of 22 abnormal patient cases

Patient Case no.	TP		FP	FN
	Closed Boundary Lesion Detection	Bone Deformation Lesion Detection		
1				
2				
3				
4				

Patient Case no.	TP		FP	FN
	Closed Boundary Lesion Detection	Bone Deformation Lesion Detection		
5				
6				
7				
8				
9				

Patient Case no.	TP		FP	FN
	Closed Boundary Lesion Detection	Bone Deformation Lesion Detection		
10				
11				
12				
13				
14				

Patient Case no.	TP		FP	FN
	Closed Boundary Lesion Detection	Bone Deformation Lesion Detection		
15				
16				
17				
18				
19				

Patient Case no.	TP		FP	FN
	Closed Boundary Lesion Detection	Bone Deformation Lesion Detection		
20				
21				
22				

REFERENCES

1. Tracy, K.D., et al., *Utility and effectiveness of computer-aided diagnosis of dental caries*. General Dentistry, 2011. **59**(2): p. 136-144.
2. Institute, N.C. *Cancer statistics*. 2015 [cited 2015 03/30]; Available from: <http://seer.cancer.gov/statfacts/html/oralcav.html>.
3. Dental, W.F. [cited 2015 03/31]; Available from: <http://www.wichitafamilydental.com/cone-beam-ct-scan/>.
4. Li, S., et al., *Semi-automatic computer aided lesion detection in dental X-rays using variational level set*. Pattern Recognition, 2007. **40**(10): p. 2861-2873.
5. Gakenheimer, D.C., et al., *Quantitative dental caries detection system and method*. 1997, Google Patents.
6. Gakenheimer, D.C., *The efficacy of a computerized caries detector in intraoral digital radiography*. Journal of the American Dental Association, 2002. **133**(7): p. 883-890.
7. Gakenheimer, D.C., et al., *Advancements in automated dental caries detection using DICOM image files*, in *International Congress Series*. 2005. p. 1250-1255.
8. Firestone, A.R., et al., *The Effect of a Knowledge-Based, Image Analysis and Clinical Decision Support System on Observer Performance in the Diagnosis of Approximal Caries from Radiographic Images*. Caries Research, 1998. **32**(2): p. 127-134.
9. Olsen, G.F., et al. *An image-processing enabled dental caries detection system*. in *2009 ICME International Conference on Complex Medical Engineering, CME 2009*. 2009.
10. Kavitha, M.S., et al., *Diagnosis of osteoporosis from dental panoramic radiographs using the support vector machine method in a computer-aided system*. BMC Medical Imaging, 2012. **12**.
11. Muramatsu, C., et al., *Automated measurement of mandibular cortical width on dental panoramic radiographs*. International Journal of Computer Assisted Radiology and Surgery, 2013. **8**(6): p. 877-885.
12. Reddy, T.K. and N. Kumaravel, *Multi resolution based texture analysis of jaw bone lesions*. European Journal of Scientific Research, 2011. **51**(3): p. 415-423.
13. van der Stelt, P.F. and W.G.M. Geraets, *Computer-aided interpretation and quantification of angular periodontal bone defects on dental radiographs*. IEEE Transactions on Biomedical Engineering, 1991. **38**(4): p. 334-338.
14. Kapur, J.N., P.K. Sahoo, and A.K. Wong, *A new method for gray-level picture thresholding using the entropy of the histogram*. Computer vision, graphics, and image processing, 1985. **29**(3): p. 273-285.

15. Li, C.H. and P.K.S. Tam, *An iterative algorithm for minimum cross entropy thresholding*. Pattern Recognition Letters, 1998. **19**(8): p. 771-776.
16. Glasbey, C.A., *An Analysis of Histogram-Based Thresholding Algorithms*. CVGIP: Graphical Models and Image Processing, 1993. **55**(6): p. 532-537.
17. Kittler, J. and J. Illingworth, *Minimum error thresholding*. Pattern Recognition, 1986. **19**(1): p. 41-47.
18. Prewitt, J.M.S. and M.L. Mendelsohn, *THE ANALYSIS OF CELL IMAGES**. Annals of the New York Academy of Sciences, 1966. **128**(3): p. 1035-1053.
19. Tsai, W.-H., *Moment-preserving thresholding: a new approach*, in *Document image analysis*, O.G. Lawrence and K. Rangachar, Editors. 1995, IEEE Computer Society Press. p. 44-60.
20. Otsu, N., *A Threshold Selection Method from Gray-Level Histograms*. IEEE Transactions on Systems, Man, and Cybernetics, 1979. **9**(1): p. 62-66.
21. Doyle, W., *Operations Useful for Similarity-Invariant Pattern Recognition*. J. ACM, 1962. **9**(2): p. 259-267.
22. Shanbhag, A.G., *Utilization of Information Measure as a Means of Image Thresholding*. CVGIP: Graphical Models and Image Processing, 1994. **56**(5): p. 414-419.
23. Zack, G.W., W.E. Rogers, and S.A. Latt, *Automatic measurement of sister chromatid exchange frequency*. J Histochem Cytochem, 1977. **25**(7): p. 741-53.
24. Jui-Cheng, Y., C. Fu-Juay, and C. Shyang, *A new criterion for automatic multilevel thresholding*. Image Processing, IEEE Transactions on, 1995. **4**(3): p. 370-378.
25. Sahoo, P.K., S. Soltani, and A.K.C. Wong, *A survey of thresholding techniques*. Computer Vision, Graphics, and Image Processing, 1988. **41**(2): p. 233-260.
26. Gonzalez, R.C. and R.E. Woods, *Digital Image Processing*. 1992: Addison-Wesley Longman Publishing Co., Inc. 716.
27. Haralick, R.M. and L.G. Shapiro, *Computer and Robot Vision*. 1992: Addison-Wesley Longman Publishing Co., Inc. 630.
28. Haralick, R.M., K. Shanmugam, and I.H. Dinstein, *Textural Features for Image Classification*. Systems, Man and Cybernetics, IEEE Transactions on, 1973. **SMC-3**(6): p. 610-621.
29. Clausi, D. and Y. Zhao, *Rapid co-occurrence texture feature extraction using a hybrid data structure*. Computers and Geosciences, 2002. **28**(6): p. 763-774.
30. Gebejes, A. and R. Huertas, *Texture Characterization Based on Grey-Level Co-Occurrence Matrix*. 2013.
31. Ming-Kuei, H., *Visual pattern recognition by moment invariants*. Information Theory, IRE Transactions on, 1962. **8**(2): p. 179-187.

32. Zhihu, H. and L. Jinsong. *Analysis of Hu's moment invariants on image scaling and rotation*. in *Computer Engineering and Technology (ICCET), 2010 2nd International Conference on*. 2010.
33. Jiang, J., P. Trundle, and J. Ren, *Medical image analysis with artificial neural networks*. *Computerized Medical Imaging and Graphics*, 2010. **34**(8): p. 617-631.
34. Rosenblatt, F., *Principles of neurodynamics. perceptrons and the theory of brain mechanisms*. 1961, DTIC Document.
35. LeCun, Y., et al., *Efficient BackProp*, in *Neural Networks: Tricks of the Trade*, G. Orr and K.-R. Müller, Editors. 1998, Springer Berlin Heidelberg. p. 9-50.

VITA

Shaikat Mahmood Galib was born on September, 1986, in Jhinaidaha, Bangladesh. He received his Bachelor of Science degree in Mechanical Engineering from Islamic University of Technology, Dhaka, Bangladesh in November 2008. After graduation, he worked as an Operations Engineer in NEPC Consortium Power; a 110MW barge mounted power plant in Bangladesh. He also worked in Nitol Motors Ltd; an automotive service provider of TATA Motors in Bangladesh, as a Service Executive.

Shaikat Galib joined Nuclear Engineering department as a graduate student at Missouri University of Science and Technology in August, 2013. He held a Graduate Assistantship under Dr. Hyung Koo Lee and working in the field of radiation imaging and image processing applications. He received his Master of Science in Nuclear Engineering from Missouri University of Science and technology in May, 2015